Dark and bright solitons in resonantly absorbing gratings

Tomáš Opatrný,[1,2] Boris A. Malomed,[3] and Gershon Kurizki[1]
[1]*Department of Chemical Physics, Weizmann Institute of Science, 76100 Rehovot, Israel*
[2]*Department of Theoretical Physics, Palacký University, Svobody 26, 779 00 Olomouc, Česko*
[3]*Department of Interdisciplinary Studies, Faculty of Engineering, Tel Aviv University, Tel Aviv 69978, Israel*
(Received 25 May 1999)

We consider an optical medium consisting of a periodic refractive-index grating and a periodic set of thin layers of two-level systems resonantly interacting with the electromagnetic field. Recently, it has been shown that such a system gives rise to a vast variety of stable bright solitons. In this work, we demonstrate that the system has another very unusual property: stable bright solitons can coexist with stable continuous-wave (cw) states and stable dark solitons (DS's). Depending on the parameters' values, a DS frequency band coexists (without overlap) with one or two bright-soliton bands. Quiescent (standing) DS's are found in an analytical form, and moving ones are obtained numerically. Simulations show that a considerable part of the DS solutions are completely stable against arbitrary small perturbations. The fact that this system supports both stable bright *and* dark solitons for the *same* parameters values may find interesting applications in photonics.
[S1063-651X(99)13311-7]

PACS number(s): 42.65.Tg, 42.25.Bs, 42.50.Gy, 78.66.−w

I. INTRODUCTION

An intriguing optical property of one-dimensionally periodic dielectric media is the existence of solitary waves in their band gaps known as ''gap solitons.'' These self-localized field structures arise due to the interplay between the medium nonlinearity and its Bragg reflections. Their spectrum is tuned away from the Bragg resonance by the nonlinearity at sufficiently high field intensities. Theoretical studies of gap solitons in Bragg gratings with Kerr nonlinearity [1] have been followed up by their experimental observation in a nonlinear optical fiber with the grating written on it [2]. Gap solitons have also been theoretically studied in gratings with second harmonic generation (SHG) [3].

A principally different mechanism of gap solitons has been revealed in a periodic array of thin layers of *resonant two-level systems* (TLS's) separated by half-wavelength nonabsorbing dielectric layers, i.e., a *resonantly absorbing Bragg reflector* (RABR) [4,5]. Such a RABR has been shown, for *any* Bragg reflectivity, to have, a vast family of stable solitons, both standing and moving [4,5]. As opposed to the 2π solitons arising in self induced transparency, i.e., resonant field – TLS interaction in a uniform medium [6], gap solitons in a RABR can have an *arbitrary* pulse area [4,5]. As shown below, gap soliton solutions can only be consistently demonstrated in a RABR with *thin* active TLS layers. By contrast, a recent attempt [7] to obtain such solutions in a periodic structure *uniformly* filled with active TLS's is physically unfounded, and fails for many parameter values.

A gap soliton is usually understood to be a moving or standing (quiescent) bright confined region, where light can freely propagate, in a dark background, where light is Bragg reflected. Along with these bright solitons, there is considerable physical interest in dark solitons (DS's), i.e., ''holes'' of a fixed shape in a continuous-wave (cw) background field of constant intensity [8]. However, no example of a stable DS has thus far been known in any periodic nonlinear medium. A principal problem is the *modulational instability* of the cw fields, i.e., the lack of a stable background to support DS's. The main innovation of the present work is that it demonstrates an unexpected property of a RABR with active layers: alongside the previously studied stable bright-soliton solutions [4,5], this system gives rise to a family of DS's, a large part of which are *stable*. While the existence of stable bright-soliton solutions along with *unstable* dark solitons is a known feature of uniform SHG media [8], the RABR with thin active layers provides, to the best of our knowledge, the first example of a nonlinear optical medium in which stable bright and dark solitons exist for the *same values* of the model's parameters (at different frequencies). We believe it is also the first example of the existence of stable bright solitons alongside *stable* cw (*background*) solutions.

The rest of this paper is organized as follows. In Sec. II we introduce the model, and analyze the spectrum of its linearized version. Properties of the standing (quiescent) bright solitons are discussed in Sec. III. Exact solutions representing quiescent DS's are obtained in Sec. IV. Section V is devoted to the crucial issue of the stability of DS's. First, we analytically consider the stability of the cw solutions, and then, by means of numerical simulations, we test the full stability of DS's. In Sec. VI, we find moving DS's by means of direct simulations, and conclude that they are drastically different from the moving DS's in the nonlinear Schrödinger equation. Effects of the finite width of the active layers are estimated in Sec. VII, experimental predictions of the work are discussed in Sec. VIII, and the conclusions are summarized in Sec. IX. In Appendixes A–F, derivations of the governing equations and of other important formulas are presented.

II. MODEL AND ITS LINEAR SPECTRUM

A. Equations of motion

As in Refs. [4] and [5], we assume a one-dimensionally periodic modulation of the linear refractive index $n(z)$ along

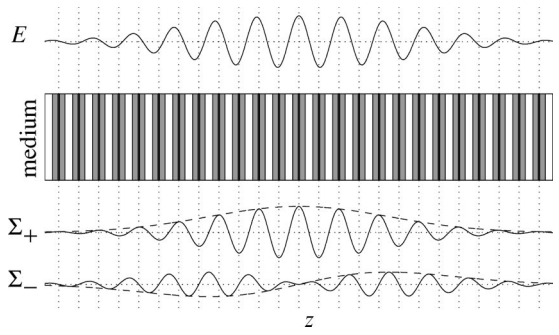

FIG. 1. Schematic description of the periodic structure and decomposition of the electric field into modes Σ_+ and Σ_-. The shading represents regions with different index of refraction; the darker the shading the larger n is. The black regions correspond to the TLS layers. The upper solid curve represents the electric field, the lower solid curves correspond to the components $\mathrm{Re}(\Sigma_+)\cos k_c z$ and $-\mathrm{Im}(\Sigma_-)\sin k_c z$, and the dashed curves are the envelopes $\mathrm{Re}(\Sigma_+)$ and $-\mathrm{Im}(\Sigma_-)$. The vertical dotted lines denote the positions of the TLS.

the z direction of the electromagnetic wave propagation (see Fig. 1). The modulation can be written as the Fourier series

$$n^2(z)=n_0^2[1+a_1\cos(2k_c z)+a_2\cos(4k_c z)+\cdots], \quad (1)$$

where n_0, a_j, and k_c are constants. For the propagation of waves whose wave vector is close to k_c, only the coefficient a_1 is essential (see Appendix B). The medium is assumed to be infinite and homogeneous in the x and y directions. The periodic grating gives rise to band gaps in the system's linear spectrum, i.e., the medium is totally reflective for waves whose frequency is inside the gaps. The central frequency of the fundamental gap is $\omega_c=k_c c/n_0$, c being the vacuum speed of light, and the gap edges are located at the frequencies

$$\omega_{1,2}=\omega_c(1\pm a_1/4), \quad (2)$$

where a_1 is the modulation depth from Eq. (1). We further assume that *very thin* TLS layers (much thinner than $1/k_c$), whose resonance frequency ω_0 is close to the gap center ω_c, are placed at the maxima of the modulated refraction index. In other words, the thin active layers are placed at the points z_{layer} such that $\cos(k_c z_{\mathrm{layer}})=\pm 1$. As discussed in Sec. VIII, quantum wells embedded in Bragg mirrors are adequately described as TLS layers.

We shall study the propagation of the electromagnetic waves with frequencies close to ω_c through the described medium. The electric field $E(z,t)$ will be decomposed into cosine and sine spatial components, having dimensionless slowly varying amplitudes Σ_+ and Σ_-, respectively,

$$E(z,t)=\hbar(\mu\tau_0)^{-1}(\mathrm{Re}[\Sigma_+(z,t)e^{-i\omega_c t}]\cos k_c z - \mathrm{Im}[\Sigma_-(z,t)e^{-i\omega_c t}]\sin k_c z), \quad (3)$$

where μ is the transition dipole moment of the TLS, and the characteristic absorption time of the field by the TLS is

$$\tau_0=n_0\mu^{-1}\sqrt{\hbar/2\pi\omega_c\varrho_0}, \quad (4)$$

ϱ_0 being the TLS density (averaged over z). As derived in Appendixes A, B, and C, the Maxwell-Bloch equations in the slowly-varying-amplitude and rotating-wave approximations yield the following set of governing equations for this system:

$$\frac{\partial^2\Sigma_+}{\partial\tau^2}-\frac{\partial^2\Sigma_+}{\partial\zeta^2}=-\eta^2\Sigma_++2i\eta P+2\frac{\partial P}{\partial\tau}, \quad (5)$$

$$\frac{\partial^2\Sigma_-}{\partial\tau^2}-\frac{\partial^2\Sigma_-}{\partial\zeta^2}=-\eta^2\Sigma_--2\frac{\partial P}{\partial\zeta}, \quad (6)$$

$$\frac{\partial P}{\partial\tau}=-i\delta P+\Sigma_+ w, \quad (7)$$

$$\frac{\partial w}{\partial\tau}=-\mathrm{Re}(\Sigma_+P^*), \quad (8)$$

where P is the dimensionless slow-varying polarization normalized as $|P|\leqslant 1$, and w is the TLS population inversion ranging between -1 and $+1$. Here, we have neglected losses and the finite width of the active layers, which are analyzed in Sec. VII and Appendixes D and E. The dimensionless time τ, coordinate ζ, and detuning δ are defined as follows:

$$\tau\equiv t/\tau_0, \quad \zeta\equiv(n_0/c\tau_0)x, \quad \delta\equiv(\omega_0-\omega_c)\tau_0. \quad (9)$$

The dimensionless modulation strength η in Eqs. (5) and (6) is the ratio of the TLS absorption distance to the Bragg reflection distance, which can be expressed as

$$\eta=\frac{a_1\omega_c\tau_0}{4}. \quad (10)$$

Note that Σ_- does not influence the evolution of Σ_+, P and w, but is driven by $\partial P/\partial\zeta$.

Combining Eqs. (7) and (8), one can eliminate the TLS population inversion:

$$w=\pm\sqrt{1-|P|^2}. \quad (11)$$

Without the field-induced polarization, the TLS population is not inverted ($w=-1$), hence the lower sign must be chosen in Eq. (11). Thus the remaining equations for Σ_+ and P form a *closed system*,

$$\frac{\partial^2\Sigma_+}{\partial\tau^2}-\frac{\partial^2\Sigma_+}{\partial\zeta^2}=-\eta^2\Sigma_++2i(\eta-\delta)P-2\sqrt{1-|P|^2}\Sigma_+, \quad (12)$$

$$\frac{\partial P}{\partial\tau}=-i\delta P-\sqrt{1-|P|^2}\Sigma_+, \quad (13)$$

and Σ_-, the field component driven by $\partial P/\partial\zeta$, can then be found from Eq. (6).

We emphasize again the crucial role of the assumption that the TLS layers are *much thinner than a wavelength* and satisfy the Bragg condition. Without this assumption we could not have obtained Eqs. (5) – (8) which are closed in P

and w. This makes the present analysis principally at variance with Ref. [7], where the active medium is assumed to be uniform, although (see Appendixes D and E and Sec. VII) closed equations of motion *cannot* be obtained then. Furthermore, highly nontrivial field structures can evolve in a uniformly doped medium [9], due to higher order Fourier components of the polarization, which are omitted in Ref. [7]. We finally note that the model of Ref. [10], i.e., a periodic array of thin TLS layers *without* modulation of the linear index of refraction, corresponds to system (5) – (8) with $\eta=0$, and gives rise to a different dynamics.

B. Energy densities

To see the physical meaning of the quantities $\Sigma_{\pm}$ and P, we express the energy density of the electromagnetic field as

$$W_F=(1/8)\hbar\omega_c\rho_0(|\Sigma_+|^2+|\Sigma_-|^2), \tag{14}$$

that of the TLS excitations as

$$W_A=(1/2)\hbar\omega_0\rho_0(1-\sqrt{1-|P|^2}), \tag{15}$$

and the energy density of the TLS-field interaction as

$$W_I=(1/2)\hbar\rho_0\tau_0^{-1}\mathrm{Im}(\Sigma_+P^*). \tag{16}$$

From Eq. (14) we conclude that $|\Sigma_+|^2$ and $|\Sigma_-|^2$ are proportional to the number of photons per TLS (atom), in the standing-wave symmetric and antisymmetric modes whose antinodes and nodes, respectively, coincide with the active layers (see Fig. 1). Since the interaction time τ_0 [see Eq. (4)] is usually much larger than the optical period $2\pi/\omega_c$, the interaction energy is negligible in comparison to the energies of the field and atomic excitations.

C. Linearized spectrum

Before studying the consequences of the system nonlinearity, it is important to consider the spectrum produced by the linearized version of Eqs. (6), (12), and (13). Setting $w=-1$, and

$$\Sigma_+=Ae^{i(\kappa\zeta-\chi\tau)}, \tag{17}$$

$$\Sigma_-=Be^{i(\kappa\zeta-\chi\tau)}, \tag{18}$$

$$P=Ce^{i(\kappa\zeta-\chi\tau)}, \tag{19}$$

from the linearized equation (13) we obtain that $C=i(\delta-\chi)^{-1}A$. Substituting this into Eqs. (6) and (12), we arrive at the dispersion relation for the wave number κ and frequency χ in the form

$$(\chi^2-\kappa^2-\eta^2)(\chi-\delta)\{(\chi-\delta)[\chi^2-\kappa^2-(2+\eta^2)] +2(\eta-\delta)\}=0. \tag{20}$$

Different branches of the dispersion relation generated by Eq. (20) are shown in Fig. 2. The roots $\chi=\pm\sqrt{\kappa^2+\eta^2}$ (corresponding to the solid lines in Fig. 2) originate from the driven equation (6) and represent the dispersion relation of the Bragg reflector with the gap $|\chi|<\eta$ [cf. Eq. (2)], that does not ''feel'' the interaction with the active layers. The degenerate root $\chi\equiv\delta$ is trivial, as it corresponds to the eigenmode (19) with $A=B=0$. The important roots are those of the expression in the curled brackets in Eq. (20) (shown by the dashed and dash-dotted lines in Fig. 1), since they give rise to the nontrivial spectral features to be studied here. They will be shown below to correspond to bright or dark solitons in the indicated (shaded) bands.

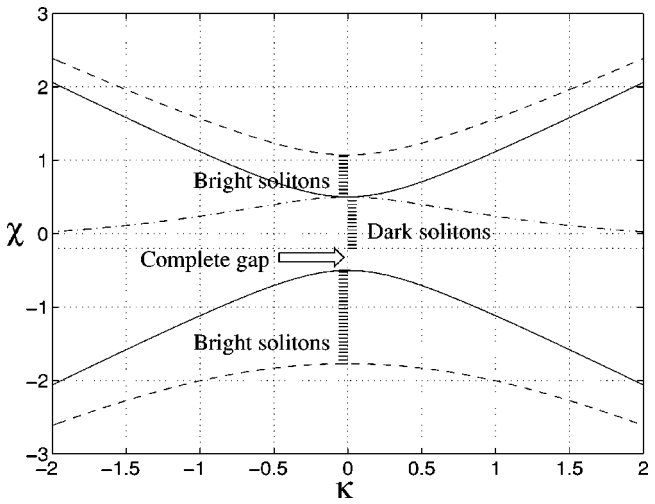

FIG. 2. The dispersion curves (dimensionless frequency χ vs dimensionless wave vector k) at $\eta=0.5$ and $\delta=-0.2$. The solid lines show the dispersion branches corresponding to the ''bare'' (noninteracting) grating, while the dashed and dash-dotted lines stand for the dispersion branches of the grating ''dressed'' by the active medium. The frequency bands that support the standing dark and bright solitons are shaded. The arrow indicates a complete gap, where no field propagation takes place.

III. BRIGHT SOLITONS

Stationary solutions of Eqs. (12) and (13) corresponding to bright solitons were derived in Ref. [5]. Let us first recapitulate the main results. Stationary solutions for the symmetric-mode field Σ_+ and polarization P are sought in the forms

$$\Sigma_+=e^{-i\chi\tau}\mathcal{S}(\zeta), \quad P=ie^{-i\chi\tau}\mathcal{P}(\zeta), \tag{21}$$

with real $\mathcal{P}$ and $\mathcal{S}$. Substituting this into Eq. (13), we eliminate $\mathcal{P}$ in favor of $\mathcal{S}$,

$$\mathcal{P}=-\frac{\mathrm{sgn}(\chi-\delta)\mathcal{S}}{\sqrt{(\chi-\delta)^2+|\mathcal{S}|^2}}, \tag{22}$$

and obtain an equation for $\mathcal{S}(\zeta)$,

$$\mathcal{S}''=(\eta^2-\chi^2)\mathcal{S}-2\mathcal{S}\frac{(\eta-\chi)\mathrm{sgn}(\chi-\delta)}{\sqrt{(\chi-\delta)^2+\mathcal{S}^2}}, \tag{23}$$

where the prime stands for $d/d\zeta$. Equation (23) can be cast into the form of Newton's equation of motion for a particle with coordinate $\mathcal{S}(\zeta)$ moving in a potential $U(\mathcal{S})$,

$$\mathcal{S}''=-U'(\mathcal{S}), \tag{24}$$

where

$$U(\mathcal{S}) = -\tfrac{1}{2}(\eta^2-\chi^2)\mathcal{S}^2 + 2(\eta-\chi) \times \mathrm{sgn}(\chi-\delta)\sqrt{(\chi-\delta)^2+\mathcal{S}^2}. \quad (25)$$

The potential will give rise to bright solitons, provided it has two symmetric minima [5]. As follows from Eq. (25), the latter condition implies that the quadratic part of the potential is concave, i.e., $|\chi|>\eta$, and the second (asymptotically linear) part of expression (25) is convex, so that $\chi<\delta$. Moreover, two minima separated by a local maximum in $\mathcal{S}=0$ appear if $U''(0)<0$. From this inequality it follows that bright solitons can appear in two frequency bands χ, the lower band being

$$\chi_1<\chi<\min\{\chi_2,-\eta,\delta\}, \quad (26)$$

and the upper band

$$\max\{\chi_1,\eta,\delta\}<\chi<\chi_2, \quad (27)$$

where the boundary frequencies $\chi_{1,2}$ are given by

$$\chi_{1,2}\equiv(1/2)[\,\delta-\eta\mp\sqrt{(\eta+\delta)^2+8}\,]. \quad (28)$$

The lower band exists for all values $\eta>0$ and δ, while the upper one only exists for

$$\delta>\eta-1/\eta, \quad (29)$$

which follows from the requirement $\chi_2>\eta$ [see Eq. (27)].

The bright soliton corresponds to the solution of the Newton equation (24) with the ''particle'' sitting at time $-\infty$ on the local maximum $\mathcal{S}=0$, then swinging to one side and finally returning to $\mathcal{S}=0$ at time $+\infty$. Such solutions have been found in an implicit form in Ref. [5]:

$$\mathcal{S}(\zeta)=2|\chi-\delta|\mathcal{R}(\zeta)(1-\mathcal{R}^2(\zeta))^{-1}, \quad (30)$$

with

$$|\zeta| = \sqrt{2\left|\frac{\chi-\delta}{\chi-\eta}\right|}\left[(1-\mathcal{R}_0^2)^{-1/2}\tan^{-1}\sqrt{\frac{\mathcal{R}_0^2-\mathcal{R}^2}{1-\mathcal{R}_0^2}} + (2\mathcal{R}_0)^{-1}\ln\left(\frac{\mathcal{R}_0+\sqrt{\mathcal{R}_0^2-\mathcal{R}^2}}{\mathcal{R}}\right)\right] \quad (31)$$

and

$$\mathcal{R}_0^2 = 1-\frac{|(\chi+\eta)(\chi-\delta)|}{2}. \quad (32)$$

The polarization amplitude $\mathcal{P}$ is determined by $\mathcal{S}$ via Eq. (22).

To calculate the electric field in the antisymmetric Σ_- mode, we substitute

$$\Sigma_- = ie^{-i\chi\theta}\mathcal{A}(\zeta) \quad (33)$$

into Eq. (6), and obtain

$$\mathcal{A}''+(\chi^2-\eta^2)\mathcal{A}=2\mathcal{P}', \quad (34)$$

which can be easily solved by the Fourier transform, once $\mathcal{P}(\zeta)$ is known. An example of bright solitons is depicted in Fig. 3. Note that, depending on the parameters η, δ, and χ, the main part of the soliton's energy can be carried by either the Σ_+ or Σ_- mode.

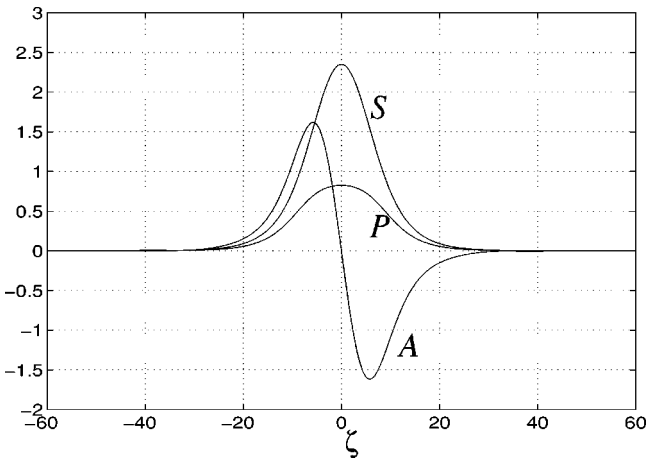

FIG. 3. A typical example of a bright soliton. The variables $\mathcal{S}$, $\mathcal{P}$, and $\mathcal{A}$ are plotted as functions of ζ for the parameters $\eta=0.2$, $\delta=-2$, and $\chi=0.4$.

Thus far we have been dealing with standing (quiescent) solitons. To obtain moving solitons, the following procedure has been used in Ref. [5]. The standing-soliton solution has been multiplied by a factor $\exp(i\kappa\zeta)$, i.e., the soliton solution has been used as a modulation for a plane wave. It has been numerically shown that such structures are stable and move with a κ-dependent velocity.

IV. DARK SOLITONS

Dark solitons are obtained similarly to the bright ones, by solving Eq. (24) with potential (25). The potential will give rise to DS's provided that it has two symmetric maxima. In this case the quadratic part of the potential is convex, i.e., $|\chi|<\eta$, and the second (asymptotically linear) part of expression (25) is concave, so that $\chi>\delta$. From these two inequalities, a simple necessary restriction on the model's parameters follows

$$\delta<\eta. \quad (35)$$

The condition for the existence of the symmetric maxima determines the following frequency interval χ (recall that η is defined to be positive):

$$\max\{\delta,-\eta\}<\chi<\min\{\chi_2,\eta\}, \quad (36)$$

Making use of Eq. (28), one can easily check, once condition (35) is satisfied, that the DS-supporting band (36) *always* exists. The DS frequency range defined by Eq. (36) is marked by shading (to the right from zero) in Fig. 2. The maxima of the potential are located at the points

$$\mathcal{S}_M=\pm\sqrt{4(\eta+\chi)^{-2}-(\chi-\delta)^2}, \quad (37)$$

which correspond to the polarization values

$$\mathcal{P}_M=\mp\sqrt{1-(1/4)(\chi-\delta)^2(\chi+\eta)^2}. \quad (38)$$

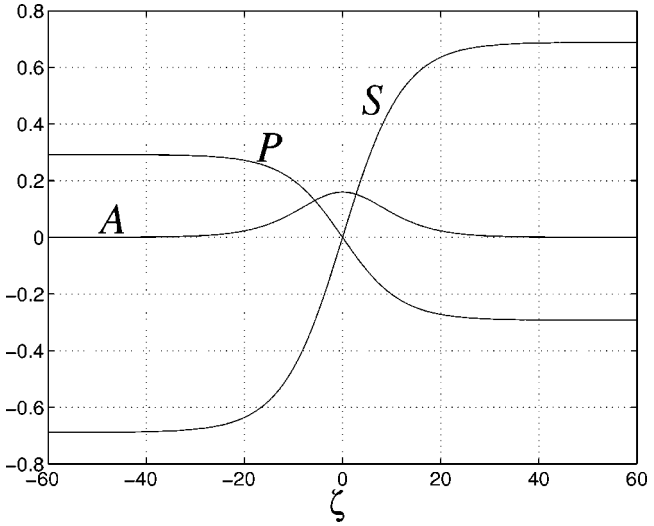

FIG. 4. A typical example of a dark soliton, presented in terms of the variables $\mathcal{S}$, $\mathcal{P}$, and $\mathcal{A}$. The parameters are $\eta=0.6$, $\delta=-2$, and $\chi=0.25$.

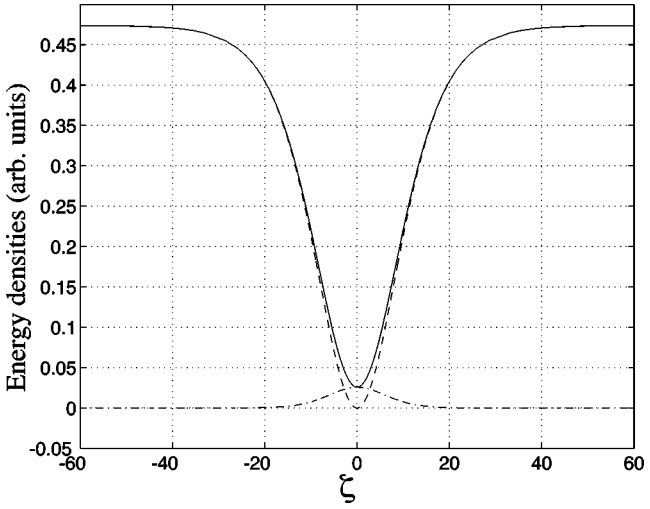

FIG. 5. Field energy densities as a function of the coordinate ζ inside the dark soliton shown in Fig. 4: $|\Sigma_+|^2$ (dashed line), $|\Sigma_-|^2$ (dash-dotted line), and their sum (continuous line).

Integrating Eq. (24) by means of energy conservation in the formal mechanical problem, we obtain $\mathcal{S}(\zeta)$ in an implicit form

$$\zeta=\pm\frac{1}{\sqrt{2}}\int_0^{\mathcal{S}}\frac{d\mathcal{S}_1}{\sqrt{U_M-U(\mathcal{S}_1)}}$$

$$\equiv\pm\frac{1}{\sqrt{2}}\int_0^{\mathcal{S}}\frac{d\mathcal{S}_1}{\sqrt{U_M+\alpha\mathcal{S}_1^2-\beta\sqrt{\gamma^2+\mathcal{S}_1^2}}}, \tag{39}$$

with

$$\alpha\equiv\tfrac{1}{2}(\eta^2-\chi^2),\quad \beta\equiv 2(\eta-\chi),\quad \gamma\equiv\chi-\delta. \tag{40}$$

Solution (39) corresponds to a trajectory connecting the potential maximum at $+\mathcal{S}_M$ in ''time'' $\zeta=\mp\infty$ to the other one at $-\mathcal{S}_M$ in ''time'' $\zeta=\pm\infty$. In terms of the Σ_+ mode of the electric field, this is exactly a quiescent (zero-velocity) DS with the background cw amplitude $\mathcal{S}_M$.

Integral (39) can be formally expressed in terms of incomplete elliptic integrals, but, practically, it is more helpful to evaluate it numerically. As in Sec. III, the polarization amplitude $\mathcal{P}$ is determined by $\mathcal{S}$ via Eq. (22), and the amplitude of the Σ_- mode is obtained by solving Eq. (34). An example of the amplitude $\mathcal{S}$ for a DS in the Σ_+ mode, together with the corresponding quantities $\mathcal{P}$ and $\mathcal{A}$, are plotted in Fig. 4.

The energy density of the $|\Sigma_+|^2$ field mode always has the shape of a hole in the background (see Fig. 5). The energy density of $|\Sigma_-|^2$ has a hump, which is the counterpart of the hole in the Σ_+ mode. The net electromagnetic energy density may have either a hole (which always exceeds zero) or a hump, depending on the system parameters η and δ and the soliton frequency χ.

As mentioned in Sec. I, a very interesting question is whether the system can support bright and dark solitons for the *same values* of the parameters. As mentioned above, DS's always exist in the frequency interval (36), once inequality (35) is satisfied. On the other hand, bright solitons are found in two frequency bands χ, given in Eqs. (26) and (27). From the discussion in Sec. III it follows that the DS frequency band *always coexists* with one or two bands supporting the bright solitons. The special case when there are *two* bright-soliton bands coexisting with the DS band is singled out by the condition

$$\eta-\frac{1}{\eta}<\delta<\eta. \tag{41}$$

One can readily check that the coexisting frequency bands supporting bright and dark solitons never overlap, i.e., quite naturally, the bright and dark solitons cannot have the same frequency.

V. STABILITY ANALYSIS

A. Background stability

An obvious necessary condition for the stability of a DS is the stability of its cw background. To tackle this problem, we use Eq. (13) to eliminate Σ_+ in favor of P,

$$\Sigma_+=-(P_\tau-i\delta P)(1-|P|^2)^{-1/2}, \tag{42}$$

and insert it into Eq. (12). The resulting equation for P is linearized around the stationary value $\mathcal{P}_M$ [see Eq. (38)], substituting

$$P=\mathcal{P}_M e^{-i\chi\tau}[1+a(\zeta,\tau)+ib(\zeta,\tau)], \tag{43}$$

where a and b are small real perturbations. We thus obtain a cumbersome system of linear real equations for a and b, which is not displayed here. It is convenient to look for its general solution in the form [cf. Eq. (19)],

$$a(\zeta,\tau)=a_0 e^{i(\kappa\zeta-\Omega\tau)},\quad b(\zeta,\tau)=b_0 e^{i(\kappa\zeta-\Omega\tau)}, \tag{44}$$

which leads to a dispersion relation for Ω and κ, that consists of two parts:

$$-(\chi-\delta)(\chi+\eta)^2\Omega^3-2[\chi(\chi-\delta)(\chi+\eta)^2+2]\Omega^2$$
$$+[(\eta+\chi)^3(\eta-\delta)(\chi-\delta)-8\chi$$
$$+(\chi-\delta)(\chi+\eta)^2\kappa^2]\Omega$$
$$+(\eta^2-\chi^2)[4-(\chi-\delta)^2(\eta+\chi)^2]+4\kappa^2=0 \quad (45)$$

and

$$-\Omega^3-(3\chi-\delta)\Omega^2+[(\eta-\chi)(2\chi+\eta-\delta)+\kappa^2]\Omega$$
$$+(\chi-\delta)\kappa^2=0. \quad (46)$$

We have checked numerically that, for many values of η, δ, and χ that support DS's according to the results obtained in Sec. IV all the roots of Eqs. (45) and (46) are real for *any* real κ. This implies the stability of the background for these values of η, δ, and χ. We have never found any values compatible with the existence of DS that would give rise to a background instability.

Equations (45) and (46) represent dispersion relations which are valid under the condition of strong background field $\mathcal{S}_M$, and then replace the zero-field dispersion relations of Eq. (20). This kind of optical bistability can be compared to the distributed feedback bistability with Kerr nonlinearity studied in Ref. [11].

B. Direct numerical stability tests

Even though there is no evidence of background instability, we have to simulate the full system of the partial differential equations, in order to directly test the DS stability. We have numerically integrated Eqs. (12) and (13), with the initial condition differing from the exact DS solution by a small perturbation added to it. Two different kinds of small perturbations have been tested: (i) a spatially extended random noise added independently to Σ_+ and P, and (ii) a localized perturbation in the form of a Gaussian multiplied by $\exp(i\kappa\zeta)$, added to the field Σ_+.

The results are strongly dependent on the parameters η, δ, and χ: for some values we have observed an explosion of the initial perturbation, leading to a completely irregular pattern, whereas for others the DS shape has *remained virtually undisturbed*. The dependence of the stability on the parameters η and χ with fixed δ is shown in Fig. 6. The darkest area of the DS parameter region corresponds to the stable regime where no instability has occurred during the entire simulation time (typically, $\tau\sim 500$). In the rest of the parameter region, DS are unstable: in the lightest part of the DS's region, the instability develops very quickly (at $\tau<50$), whereas in the intermediate part the instability builds up relatively slow. As can be seen, the unstable behavior occurs closer to the boundaries of the existence region, $\chi=\pm\eta$ and $\chi=\delta$, whereas along the boundary $\chi=\chi_2$ (corresponding to the DS-supporting background which degenerates into the trivial zero solution), DS's are stable.

A typical example of the stable behavior is displayed in Fig. 7: an initial perturbation pulse splits and propagates across the DS without affecting it. In plotting the figure we have used the (time dependent) envelopes $\mathcal{S}$, $\mathcal{A}$, and $\mathcal{P}$ without the oscillatory part $\exp(-i\chi\tau)$, i.e.,

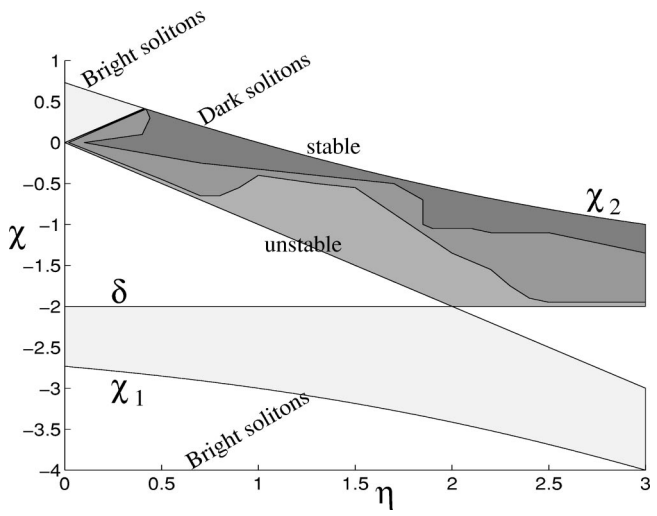

FIG. 6. Parameter regions (η vs χ) for dark [Eq. (36)] and bright [Eqs. (26) and (27)] solitons at $\delta=-2$. The boundaries χ_1 and χ_2 are given by Eq. (28). In the DS region, the darkest area corresponds to stable behavior, whereas in the remaining part the (numerical) solutions are unstable: in the lightest area (of DS's) instability develops very quickly, while in the intermediate area the DS exists for a much longer time before the onset of the instability.

$$\Sigma_+=\exp(-i\chi\tau)\mathcal{S}(\zeta,\tau), \quad (47)$$

$$\Sigma_-=i\exp(-i\chi\tau)\mathcal{A}(\zeta,\tau), \quad (48)$$

$$P=i\exp(-i\chi\tau)\mathcal{P}(\zeta,\tau). \quad (49)$$

VI. MOVING DARK SOLITONS

Thus far we have considered only quiescent DS's. A challenging question is whether they also have moving counterparts. Adding the velocity parameter to the exact DS solution is not trivial, as the underlying equations (12) and (13) have no Galilean or Lorentzian invariance. The physical reason for this is the existence of the special (laboratory) reference frame, in which the Bragg grating is at rest. In principle we can, in analogy to the stationary solutions and Eq. (21), substitute functions of the argument $(\zeta-v\tau)$ into the set equations (12) and (13) to obtain an ordinary differential equation. However this equation is a complicated complex nonlinear equation of the third order, containing all the lower derivatives, so that we could not take the advantage of the Newton-like structure as in Secs. III and IV. Though it is possible to solve such an equation numerically, we have chosen to deal with the original set of partial differential equations to better understand the nature of the evolution.

As a first attempt, suggested by the analogy with the classical DS's in the nonlinear Schrödinger (NLS) equation, we have tried to generate the moving solitons by multiplying, in the initial conditions, the quiescent DS's by a factor proportional to $\exp(i\kappa\zeta)$, thus assuming a traveling-wave cw background. The exact traveling-wave cw solutions can easily be found by suitably generalizing substitutions (21) in the system os equations (12) and (13). However, this approach has never produced a moving DS.

It has proven possible to generate stable moving DS's from quiescent ones in a different way. To this end, recall

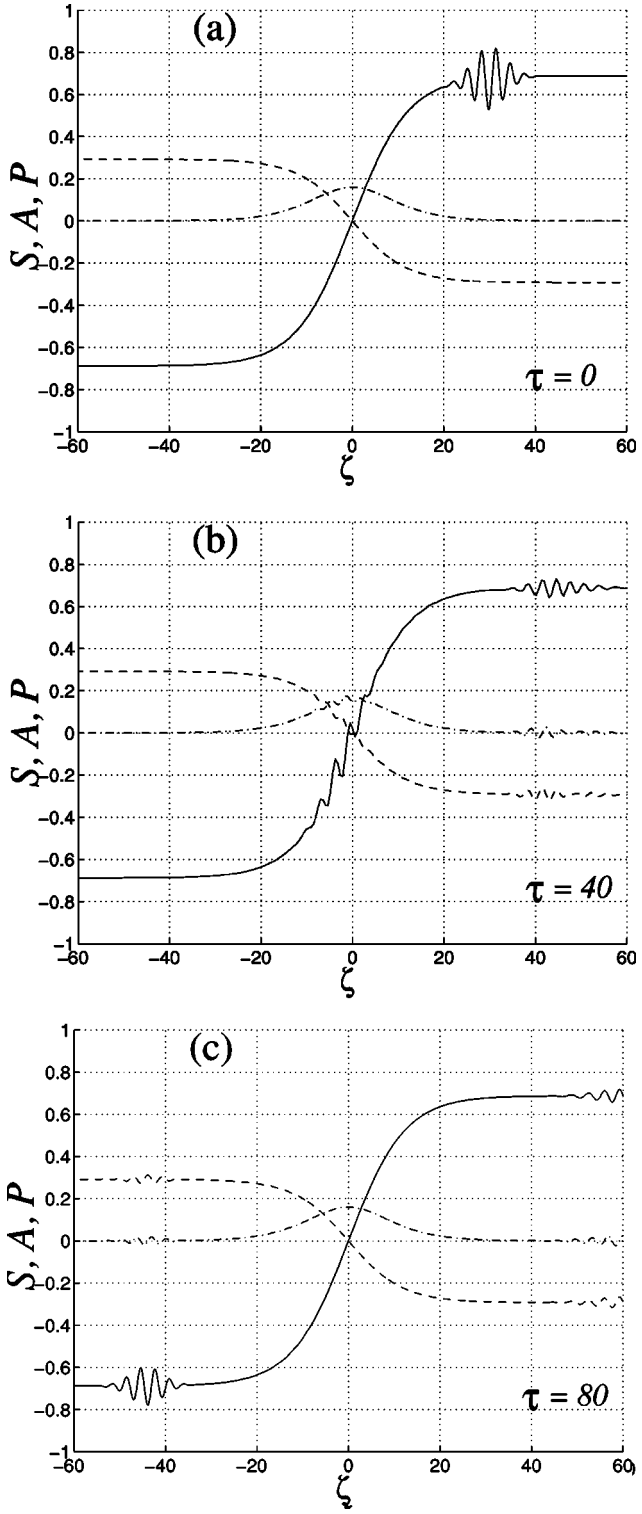

FIG. 7. Evolution of a dark soliton with a superimposed perturbation. The parameters take the same values as in Fig. 4. The continuous line is Re($\mathcal{S}$), the dashed line is Re($\mathcal{P}$), and the dash-dotted line is Re($\mathcal{A}$). Plots (a), (b), and (c) correspond, to the initial conditions ($\tau=0$), $\tau=40$, and $\tau=80$, respectively.

that a DS corresponds to a transition between two different values of the background cw field. The background field takes, generally, complex values [note the real values in the expressions (37) and (38) are only our choices adopted above for convenience]. The quiescent DS's correspond to a transition between two background values with phases differing by π. A principal difference of the DS's in the present model from those in the NLS equation [8] is that here a moving DS is generated by introducing a phase jump $\neq\pi$ across the DS.

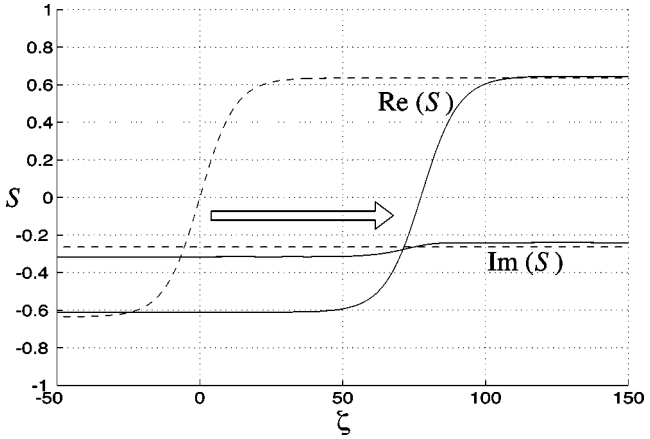

FIG. 8. Moving dark soliton: the values of the parameters are the same as in Fig. 4, the background phase-jump parameter ϕ [see Eqs. (50) and (51)] is $\phi=-\pi/4$. Dashed line: $\tau=0$; continuous line: $\tau=600$.

We have accordingly taken the initial condition for the system of equations (12) and (13) as

$$\Sigma_+(\zeta,0)=\cos\left(\frac{\phi}{2}\right)\mathcal{S}_q(\zeta)+i\sin\left(\frac{\phi}{2}\right)\mathcal{S}_M, \tag{50}$$

$$P=\cos\left(\frac{\phi}{2}\right)p_q(\zeta)+i\sin\left(\frac{\phi}{2}\right)p_M, \tag{51}$$

where $\mathcal{S}_q$ and $\mathcal{P}_q$ are the (real) functions corresponding to the quiescent DS's, $\mathcal{S}_M$ and $\mathcal{P}_M$ are given by Eqs. (37) and (38) and ϕ is the deviation from π of the background phase jump across DS's. A typical result obtained by means of this modification of the initial state is displayed in Fig. 8: the DS moves at a velocity that is proportional to ϕ. The resulting form of the moving DS is slightly different from that of the quiescent soliton. The moving DS appears to be stable over the entire simulation time. Therefore, we conclude that a local phase jump different from π is an effective way to generate moving DS's.

VII. FINITE WIDTH OF THE ACTIVE LAYERS

So far, we have assumed that TLS layers are infinitesimally thin. This assumption has allowed us to replace the infinite hierarchy of equations for different Fourier components of the TLS polarization by Eqs. (12) and (13). As shown in Appendix C, this is due to our requirement that all the TLS's be located at the antinodes of the quasi standing electromagnetic wave and thus their polarizations rotate with the same frequencies. If the envelope of the electromagnetic field varies slowly with position, so does the atomic polarization. The situation is different if the TLS's are distributed over lengths that are comparable to the wavelength: TLS's in different positions within the layer are subject to different Rabi frequencies. It is the purpose of this section and Appendix D to estimate the effect of non zero width of the active

layers which corresponds to more realistic physical situations.

We still assume the width of the active layers to be small in comparison to the wavelength. This allows us to expand the polarization as a Taylor series in the position within the layer, and consider only terms up to the second order. Averaging the polarization over the entire wavelength yields the source term of the Maxwell equations. Following the derivations in Appendixes D and E, we obtain the set of equations of motion in the forms of

$$\frac{\partial^2\Sigma_+}{\partial\tau^2}-\frac{\partial^2\Sigma_+}{\partial\zeta^2}=-\eta^2\Sigma_++2i\eta P_0+2\frac{\partial P_0}{\partial\tau}+\gamma^2\left[i\eta P_C+\frac{\partial P_C}{\partial\tau}-\frac{\partial P_B}{\partial\zeta}\right], \tag{52}$$

$$\frac{\partial^2\Sigma_-}{\partial\tau^2}-\frac{\partial^2\Sigma_-}{\partial\zeta^2}=-\eta^2\Sigma_--2\frac{\partial P_0}{\partial\zeta}+\gamma^2\left[-i\eta P_B-\frac{\partial P_C}{\partial\zeta}-\frac{\partial P_B}{\partial\tau}\right] \tag{53}$$

for the field quantities, and

$$\frac{\partial P_0}{\partial\tau}=-i\delta P_0+w_0\Sigma_+, \tag{54}$$

$$\frac{\partial P_B}{\partial\tau}=-i\delta P_B+2w_0\Sigma_--2w_1\Sigma_+, \tag{55}$$

$$\frac{\partial P_C}{\partial\tau}=-i\delta P_C+w_2\Sigma_++2w_1\Sigma_-, \tag{56}$$

$$\frac{\partial w_0}{\partial\tau}=-\frac{1}{2}\Sigma_+P_0^*+\text{c.c.}, \tag{57}$$

$$\frac{\partial w_1}{\partial\tau}=\frac{1}{2}\Sigma_-P_0^*-\frac{1}{4}\Sigma_+P_B^*-\text{c.c.}, \tag{58}$$

$$\frac{\partial w_2}{\partial\tau}=\Sigma_+\left(P_0^*-\frac{1}{2}P_C^*\right)-\frac{1}{2}\Sigma_-P_B^*+\text{c.c.} \tag{59}$$

for the TLS variables. The dimensionless parameter $\gamma\ll 1$ is proportional to the active layer width [see Appendix D for the definition, Eq. (D2)]. The new dynamical quantities are defined as

$$P_0\equiv P(z_{2j}), \tag{60}$$

$$P_B\equiv-\frac{2i}{k}\frac{\partial P}{\partial z}\Big|_{z=z_{2j}}, \tag{61}$$

$$P_C\equiv\left(\frac{1}{k^2}\frac{\partial^2}{\partial z^2}-1\right)P\Bigg|_{z=z_{2j}}, \tag{62}$$

$$w_0\equiv w(z_{2j}), \tag{63}$$

$$w_1\equiv\frac{i}{k}\frac{\partial w}{\partial z}\Bigg|_{z=z_{2j}}, \tag{64}$$

$$w_2\equiv\left(\frac{1}{k^2}\frac{\partial^2}{\partial z^2}-2\right)w\Bigg|_{z=z_{2j}}, \tag{65}$$

where z_{2j} is the position of the center of the nearest even active layer. Equations (52) – (56) with their complex conjugates, and Eqs. (57) – (59), form a closed set of 13 independent equations for the variables Σ_+, Σ_-, P_0, P_B, and P_C with their complex conjugates and w_0, w_1, and w_2, i.e., 13 real variables together. The equations are parametrized by three real parameters η, δ, and γ. Note that, for $\gamma=0$, Eqs. (52), (53), (54) and (57) are identical to Eqs. (5), (6), (7) and (8), respectively, with P_0 standing for P.

Even though the number of equations and variables has now increased, they are still relatively easy to solve numerically. They realistically express the properties of the system over quite long times. This is very important for studying the properties of *standing solitons* — it would not be true if we used a Fourier expansion of the polarization as in Ref. [7]. The problem with the treatment of Ref. [7] is that all the higher Fourier components would have enough time to develop, so that it would be impossible to adequately truncate the system of equations.

We have studied the influence of the layer width on the standing solutions. It is assumed that the change of the shape can be expanded by means of the smallness parameter γ. Considering that for $\gamma^2=0$ the quantities Σ_+ and P_0 are given by $\Sigma_+=e^{-i\chi\tau}\,\mathcal{S}(\zeta)$, and $P_0=ie^{-i\chi\tau}\,\mathcal{P}(\zeta)$, where $\mathcal{S}$ and $\mathcal{P}$ are real, we expand the quantities of the field and of the TLS's for finite γ^2 as

$$\Sigma_+=e^{-i\chi\tau}(\mathcal{S}+\gamma^2\overline{\mathcal{S}})+O(\gamma^4), \tag{66}$$

$$P_0=ie^{-i\chi\tau}(\mathcal{P}+\gamma^2\overline{\mathcal{P}})+O(\gamma^4), \tag{67}$$

$$\Sigma_-=ie^{-i\chi\tau}(\mathcal{A}+\gamma^2\overline{\mathcal{A}})+O(\gamma^4), \tag{68}$$

$$P_B=e^{-i\chi\tau}\mathcal{B}+O(\gamma^2), \tag{69}$$

$$P_C=ie^{-i\chi\tau}\mathcal{C}+O(\gamma^2). \tag{70}$$

Here $\mathcal{S}$, $\overline{\mathcal{S}}$, $\mathcal{P}$, $\overline{\mathcal{P}}$, $\mathcal{A}$, $\overline{\mathcal{A}}$, $\mathcal{B}$, and $\mathcal{C}$ are real functions of ζ. In Appendix F we derive equations for the correcting terms, which have been solved numerically.

The validity of this expansion has been checked by direct simulation of the evolution equations. The magnitude of the correcting terms varies with the system parameters, and so does the time evolution: for some values of η, δ, and χ the set of equations for finite width layers evolve into an irregular pattern, whereas for other values *the system remains stable* (e.g., for the parameters of Fig. 4).

VIII. EXPERIMENTAL CONDITIONS

The effects of TLS dephasing and deexcitation has been studied by substituting the values $-i\delta-\Gamma_2\tau_0$ for the frequency term $-i\delta$ in Eqs. (54)–(56) and the loss terms

$-\Gamma_1\tau_0(w_0+1)$ in Eq. (57), $-\Gamma_1 w_1$ in Eq. (58), and $-\Gamma_1(w_2-2)$ in Eq. (59). These modifications *have not influenced the qualitative behavior* of the solutions during times $\tau\tau_0 < 1/\Gamma_{1,2}$.

Let us now discuss the experimental conditions for the realization of the solitons, using quantum wells embedded in a semiconductor structure with periodically alternating linear index of refraction [12]. We can assume the following values: the average refraction index is $n_0 \approx 3.6$, and the wavelength (in the medium) is $\lambda \approx 232$ nm, which corresponds to the angular frequency $\omega_c \approx 2.26\times 10^{15}$ s^{-1}. Excitons in quantum wells can, under certain conditions (such as low densities, and an operating frequency close to an excitonic resonance; see Ref. [12] for details) be described as effective TLS's. We consider their surface density to be $\approx 10^{10}$–10^{11} cm^{-2}, which corresponds to a bulk density $\rho_0 \approx 10^{15}$–10^{16} cm^{-3}. If we assume that the excitons are formed by electrons and holes displaced by ≈ 1–10 nm, then the characteristic absorption time τ_0 defined in Eq. (4) is $\tau_0 \approx 10^{-13}$–10^{-12} s, and the corresponding absorption length is $c\tau_0/n_0 \approx 10$–100 μm. Thus the structures shown in Figs. 3, 4, 5, 7, and 8 occupying region of approximately 100 absorption lengths would require a device of the total width of approximately 1 mm to 1 cm, which corresponds to $\approx 10^3$–10^4 unit cells. The modulation of the refraction index can be as high as $a_1 \approx 0.3$, so that the parameter η [see Eq. (10)] can vary from 0 to 10^2. The unit of the dimensionless detuning δ would represent a 10^{-3}–10^{-2} fraction of the carrier frequency. The intensities of the applied laser field corresponding to $\Sigma_{\pm} \approx 1$ are then of the order 10^6–10^7 W/cm^2. The dephasing time discussed in [12] is $1/\Gamma_2 \approx 10^{-13}$ s, which seems to be the chief limitation of the standing soliton lifetime. Decreasing the dephasing rate appears to be the main experimental challenge.

In Ref. [12] the width of the quantum wells is considered to be 5–20 nm, which corresponds to the parameter γ^2 [see Eq. (D3)] in the range 10^{-3}–2×10^{-2}. In our simulations, taking the largest of these values and the parameters as in Fig. 4, i.e., $\eta = 0.6$, $\delta = -2$, and $\chi = 0.25$, we have observed the time evolution of the system of equations (52)–(59). As the initial condition we have taken both the DS solution corresponding to the zero width of the active layers, and the DS solution including the finite width correction as derived in Appendix F. In both cases the evolution was quite regular over the observed time $\tau \approx 50$, with the corrected solution [Eqs. (66)–(70)] remaining virtually unchanged, and the zero-width solution [quantities $\mathcal{S},\mathcal{P}$, and $\mathcal{A}$ given by Eqs. (39), (22), and (34)] starting to change after $\tau \approx 10$.

IX. DISCUSSION

An optical medium combining a periodic refractive-index grating a periodic set of thin active layers (consisting of two-level systems resonantly interacting with the field) has been investigated. Previously, it was demonstrated that this system supports a vast family of bright gap solitons [4,5]. In this work, we have shown that the system can support, depending on the initial conditions, stable dark and bright solitons for the *same values of the parameters*, which is a unique feature for nonlinear optical media. We have found zero-velocity dark solitons in an analytical form, and traveling dark solitons, with a constant phase difference ($\neq \pi$) of the background amplitudes. The latter property is a major difference from the dark solitons of the NLS equation, whose motion is supported by giving the background a nonzero wave number. Depending on the values of the parameters, the frequency band of the quiescent dark solitons coexists with one or two bands of the stable bright ones, without an overlap. Direct numerical simulations demonstrate that some dark-soliton solutions are stable against arbitrary small perturbations, whereas others are unstable, when they are close to the ''dangerous'' boundaries of their existence domain.

We have discussed the possibilities of experimental realization of such standing solitons in a semiconductor Bragg structure with quantum wells as active layers. It seems that the relatively short dephasing time is the most important limitation on their realization. It has been shown that for some values of the parameters the system evolution is only weakly influenced by the non zero width of the active layers.

ACKNOWLEDGMENTS

We thank A. Kozhekin for useful discussions. This work was supported in part by the European Union (TMR), Israel Science Foundation, and Minerva Foundation.

APPENDIX A: BLOCH EQUATIONS

We start with the Hamiltonian for a single atom in the field,

$$\hat{H} = \frac{\hbar\omega_0}{2}\hat{w} - \mathbf{E}\cdot\hat{\mathbf{d}}, \tag{A1}$$

where

$$\hat{w} \equiv |e\rangle\langle e| - |g\rangle\langle g|, \tag{A2}$$

where ω_0 is the atomic transition frequency, $|g\rangle$ and $|e\rangle$ denote the atomic ground and excited states, respectively, $\mathbf{E}$ is the electric field vector, and $\hat{\mathbf{d}}$ is the atomic dipole moment operator. We take projection on the field direction so that $\mathbf{E}\cdot\hat{\mathbf{d}} = E\hat{d}$, where

$$\hat{d} \equiv \frac{\mu}{2}(\hat{P} + \hat{P}^{\dagger}), \tag{A3}$$

μ being the dipole moment matrix element (chosen real) and

$$\hat{P} \equiv 2|g\rangle\langle e|. \tag{A4}$$

We express the electric field in a given point by means of the Rabi frequency Ω as

$$E = \frac{\hbar}{2\mu}(\Omega e^{-i\omega_c t} + \Omega^* e^{i\omega_c t}). \tag{A5}$$

Using the Heisenberg equation of motion $d\hat{A}/dt = 1/(i\hbar)[\hat{A},\hat{H}]$, defining dimensionless c numbers P and w as

$$P \equiv ie^{i\omega_c t}\langle\hat{P}\rangle, \tag{A6}$$

$$w \equiv \langle\hat{w}\rangle, \tag{A7}$$

and using the rotating wave approximation, we arrive at the Bloch equations

$$\dot{P} = -i(\omega_0 - \omega_c)P + \Omega w, \tag{A8}$$

$$\dot{w} = -\tfrac{1}{2}(\Omega P^* + \Omega^* P). \tag{A9}$$

APPENDIX B: EQUATIONS OF MOTION OF THE FIELD

We start with the Maxwell equation (one-dimensional, one component of the field vector):

$$c^2 \frac{\partial^2 E}{\partial z^2} - n^2(z)\frac{\partial^2 E}{\partial t^2} = \frac{\partial^2 P_{\rm nl}}{\partial t^2}, \tag{B1}$$

with the refraction index n modulated as in Eq. (1), E being the electric field component, and $P_{\rm nl}$ the nonlinear polarization. We use the substitution

$$E \equiv [\mathcal{E}_F(z,t)e^{ik_c z} + \mathcal{E}_B(z,t)e^{-ik_c z}]e^{-i\omega_c t} + \text{c.c.}, \tag{B2}$$

with ω_c satisfying the dispersion relation $n_0\omega_c = k_c c$ and $\mathcal{E}_F$ and $\mathcal{E}_B$ denoting the forward and the backward propagating field components. We work with the slowly varying envelope approximation assuming

$$\left|\frac{\partial^2 \mathcal{E}_{B,F}}{\partial z^2}\right| \ll \left| k_c \frac{\partial \mathcal{E}_{B,F}}{\partial z}\right|, \tag{B3}$$

$$\left|\frac{\partial^2 \mathcal{E}_{B,F}}{\partial t^2}\right| \ll \left| \omega_c \frac{\partial \mathcal{E}_{B,F}}{\partial t}\right|. \tag{B4}$$

Substituting Eq. (B2) into Eq. (B1), using Eqs. (B3) and (B4), multiplying by $e^{i(\mp k_c z + \omega_c t)}$ and averaging over the wavelength $\lambda = 2\pi/k_c$ and the period $T = 2\pi/\omega_c$, we obtain

$$\frac{c}{n_0}\frac{\partial \mathcal{E}_F}{\partial z} + \frac{\partial \mathcal{E}_F}{\partial t} = \frac{i a_1 \omega_c}{4}\mathcal{E}_B + \frac{\hbar}{2\mu\tau_0^2}P_-, \tag{B5}$$

$$-\frac{c}{n_0}\frac{\partial \mathcal{E}_B}{\partial z} + \frac{\partial \mathcal{E}_B}{\partial t} = \frac{i a_1 \omega_c}{4}\mathcal{E}_F + \frac{\hbar}{2\mu\tau_0^2}P_+, \tag{B6}$$

where we define

$$P_\pm \equiv -\frac{i\mu\tau_0^2}{\hbar\omega_c n_0^2}\left\langle \frac{\partial^2 P_{\rm nl}}{\partial t^2} e^{i(\pm k_c z + \omega_c t)}\right\rangle_{\lambda,T}, \tag{B7}$$

with τ_0 an arbitrary constant (later we take advantage of τ_0 defined as in Eq. (4)), and the averaging given as

$$\langle \cdots \rangle_{\lambda,T} \equiv \frac{1}{\lambda T}\int_\lambda \int_T \cdots dt\, dz. \tag{B8}$$

We express the field components $\mathcal{E}_{F,B}$ by means of the dimensionless quantities $\Sigma_\pm$ defined as [cf. Eqs. (3) and (B2)]

$$\mathcal{E}_{F,B} = \frac{\hbar}{4\mu\tau_0}(\Sigma_+ \pm \Sigma_-), \tag{B9}$$

and use the expressions for dimensionless position ζ and time τ given in Eq. (9) and the parameter η given in Eq. (10); differentiating the equations again with respect to ζ and τ and using some algebra, we arrive at

$$\frac{\partial^2 \Sigma_+}{\partial \tau^2} - \frac{\partial^2 \Sigma_+}{\partial \zeta^2} = -\eta^2 \Sigma_+ + i\eta(P_+ + P_-) + \frac{\partial}{\partial \tau}(P_+ + P_-) + \frac{\partial}{\partial \zeta}(P_+ - P_-) \tag{B10}$$

and

$$\frac{\partial^2 \Sigma_-}{\partial \tau^2} - \frac{\partial^2 \Sigma_-}{\partial \zeta^2} = -\eta^2 \Sigma_- + i\eta(P_+ - P_-) - \frac{\partial}{\partial \tau}(P_+ - P_-) - \frac{\partial}{\partial \zeta}(P_+ + P_-). \tag{B11}$$

APPENDIX C: NONLINEAR POLARIZATION AVERAGING: ZERO WIDTH OF TLS LAYERS

The polarization $P_{\rm nl}$ in a given point can be expressed as the dipole moment density

$$P_{\rm nl} = 4\pi\varrho\langle d\rangle = 2\pi\varrho\mu(\langle \hat{P}\rangle + \langle \hat{P}^\dagger\rangle) = -2\pi i\varrho\mu(Pe^{-i\omega_c t} - P^* e^{i\omega_c t}), \tag{C1}$$

where ϱ is the number of the two-level atoms in a unit volume. Neglecting the time derivatives of P with respect to those of $e^{-i\omega_c t}$, we can write, for the polarization derivative,

$$\frac{\partial^2 P_{nl}}{\partial t^2} = 2\pi i\omega_c^2\varrho\mu(Pe^{-i\omega_c t} - P^* e^{i\omega_c t}), \tag{C2}$$

so that $P_\pm$ on the right-hand side of Eqs. (B5) and (B6) read as

$$P_\pm = \frac{2\pi\omega_c^2\mu^2\tau_0^2}{\hbar n_0^2}\langle \varrho P e^{\pm ik_c z}\rangle_\lambda. \tag{C3}$$

Let us now assume that the density of the atoms ϱ is concentrated in zero-width layers located at z_j, such that

$$e^{ik_c z_{2j}} = 1, \quad e^{ik_c z_{2j+1}} = -1, \tag{C4}$$

i.e., it is described by

$$\varrho = \frac{\varrho_0 \lambda}{2}\sum_j \delta(z - z_j), \tag{C5}$$

where ϱ_0 is the bulk density averaged over the whole wavelength. We also assume that the space dependence of P is to a good approximation antiperiodic with respect to $\lambda/2$, i.e., $P(z + \lambda/2) \approx -P(x)$. This is in agreement with the approximate antiperiodicity of the electric field with $\lambda/2$. Denoting

by P_0 the values of P in $2j$th layers (the values in $2j+1$st layers being $-P_0$), we obtain the spatial average in Eq. (C3) as

$$P_{\pm}=\frac{2\pi\omega_c\mu^2\varrho_0\tau_0^2}{\hbar n_0^2}P_0; \tag{C6}$$

note that $P_+=P_-$ is the consequence of zero width of the layers. Defining the time τ_0 as in Eq. (4), we obtain the simple relation

$$P_{\pm}=P_0. \tag{C7}$$

Using this expression in Eqs. (B10) and (B11), we obtain the equations of motion (5) and (6) (note that the subscript 0 of P_0 has been omitted in these equations for simplicity). The equations for the polarization P_0 and inversion w_0 in the $2j$th layers can be obtained from Eqs. (A8) and (A9) by substituting for Ω [combine Eq. (3) and (A5)],

$$\Omega=\tau_0^{-1}(\Sigma_+\cos k_c z+i\Sigma_-\sin k_c z), \tag{C8}$$

and applying Eq. (C4) for the $2j$th layers positions. Expressing the detuning as in Eq. (9), we obtain the equations of motion (7) and (8).

APPENDIX D: NONLINEAR POLARIZATION AVERAGING: FINITE WIDTH OF TLS LAYERS

Let us assume that the TLS density is given, instead of Eq. (C5), by

$$\varrho=\frac{\varrho_0\lambda}{2}f(x), \tag{D1}$$

where ϱ_0 is the density averaged over the whole wavelength and the function $f(z)$ has the properties

$$f(z)\geqslant 0,\quad f(z+\lambda/2)=f(z),$$

$$\int_{z_j-(\lambda/4)}^{z_j+(\lambda/4)}f(z)dz=1,$$

$$\int_{z_j-(\lambda/4)}^{z_j+(\lambda/4)}zf(z)dz=0,$$

$$\int_{z_j-(\lambda/4)}^{z_j+(\lambda/4)}z^2f(z)dz=\frac{\gamma^2}{k^2}, \tag{D2}$$

where $\gamma\ll 1$ is a dimensionless parameter describing the thickness of the layers. Note that for a rectangular f of the width D this parameter is

$$\gamma^2=\frac{\pi^2D^2}{3\lambda^2}. \tag{D3}$$

To calculate $\langle\varrho Pe^{\pm ik_cz}\rangle_\lambda$ of Eq. (C3), we expand the spatial dependence of P and $\exp(\pm ik_cz)$ in Taylor series,

$$\begin{aligned}\langle\varrho Pe^{\pm ik_cz}\rangle_\lambda=e^{\pm ik_cz_{2j}}\varrho_0\int_{z_{2j}-(\lambda/4)}^{z_{2j}+(\lambda/4)}f(z)\\ \times\left[P_0+P_0'(z-z_{2j})+\frac{1}{2}P_0''(z-z_{2j})^2+\cdots\right]\\ \times\left[1\pm ik_c(z-z_{2j})-\frac{k_c^2}{2}(z-z_{2j})^2+\cdots\right]dz,\end{aligned} \tag{D4}$$

where P_0, P_0', and P_0'' refer to the value of P, and its spatial first and second derivatives at $z=z_{2j}$. Neglecting higher than quadratic terms and using the properties of $f(z)$ [Eq. (D2)], we arrive at

$$\langle\varrho Pe^{\pm ik_cz}\rangle_\lambda\approx\varrho_0\left[P_0+\gamma^2\left(\frac{P_0''}{2k^2}\pm\frac{iP_0'}{k}-\frac{P_0}{2}\right)\right], \tag{D5}$$

so that

$$P_{\pm}\approx P_0+\gamma^2\left(\frac{P_0''}{2k^2}\pm\frac{iP_0'}{k}-\frac{P_0}{2}\right). \tag{D6}$$

Using these values in Eq. (C3), substituting into Eqs. (B10) and (B11), and considering the definitions (60)–(62), we obtain the field equations of motion in the form of Eqs. (52) and (53).

APPENDIX E: EQUATIONS OF MOTION FOR ATOMIC PARAMETERS IN FINITE-WIDTH TLS LAYERS

We use Eq. (C8) for Ω in (A8) and (A9) to write the Bloch equations in a point z as

$$\frac{\partial P}{\partial\tau}=-i\delta P+[\cos(k_cz)\Sigma_++i\sin(k_cz)\Sigma_-]w, \tag{E1}$$

$$\frac{\partial w}{\partial\tau}=-\frac{1}{2}[\cos(k_cz)\Sigma_++i\sin(k_cz)\Sigma_-]P^*+\text{c.c.} \tag{E2}$$

Taking into account that the spatial derivatives of $\Sigma_\pm$ are much smaller than those of $\sin(k_cz)$ and $\cos(k_cz)$, and calculating the first and second derivatives in the point $z=z_{2j}$, we obtain

$$\frac{\partial P_0}{\partial\tau}=-i\delta P_0+\Sigma_+w_0, \tag{E3}$$

$$\frac{\partial P_0'}{\partial\tau}=-i\delta P_0'+ik_c\Sigma_-w_0+\Sigma_+w_0', \tag{E4}$$

$$\frac{\partial P_0''}{\partial\tau}=-i\delta P_0''-k_c^2\Sigma_+w_0+2ik_c\Sigma_-w_0'+\Sigma_+w_0'' \tag{E5}$$

and

$$\frac{\partial w_0}{\partial\tau}=-\frac{1}{2}\Sigma_+P_0^*+\text{c.c.}, \tag{E6}$$

$$\frac{\partial w_0'}{\partial \tau} = -\frac{ik_c}{2}\Sigma_- P_0^* - \frac{1}{2}\Sigma_+ P_0'^* + \text{c.c.}, \tag{E7}$$

$$\frac{\partial w_0''}{\partial \tau} = \frac{k_c^2}{2}\Sigma_+ P_0^* - ik_c\Sigma_- P_0'^* - \frac{1}{2}\Sigma_+ P_0''^* + \text{c.c.} \tag{E8}$$

Using definitions (60)–(65), we arrive at the equations of motion (54)–(59).

APPENDIX F: CORRECTIONS TO STANDING SOLITON SOLUTIONS WITH FINITE-WIDTH TLS LAYERS

Let us express w_0 up to the second order, and w_1 and w_2 up to the zeroth order in γ. We start from the requirement

$$w^2(z) + P(z)P^*(z) = 1, \tag{F1}$$

expand w and P in a Taylor series in z_{2j},

$$w(z) = w_0 + w_0'(z - z_{2j}) + \frac{w_0''}{2}(z - z_{2j})^2 + \cdots, \tag{F2}$$

$$P(z) = P_0 + P_0'(z - z_{2j}) + \frac{P_0''}{2}(z - z_{2j})^2 + \cdots, \tag{F3}$$

and compare the terms with equal powers of $(z - z_{2j})$, then use Eqs. (60)–(65) to change from w_0', w_0'', P_0', and P_0'' to w_1, w_2, P_C, and P_B, and substitute for P_0, P_C, and P_B from (67), (69), and (70). We thus obtain

$$w_0 = -\sqrt{1-\mathcal{P}^2} + \frac{\mathcal{P}\overline{\mathcal{P}}}{\sqrt{1-\mathcal{P}^2}}\gamma^2 + O(\gamma^4), \tag{F4}$$

$$w_1 = i\frac{\mathcal{P}\mathcal{B}}{2\sqrt{1-\mathcal{P}^2}} + O(\gamma^2), \tag{F5}$$

$$w_2 = \frac{8 + \mathcal{B}^2 - 12\mathcal{P}^2 + 4\mathcal{P}^4 + 4\mathcal{P}\mathcal{C}(1-\mathcal{P}^2)}{4(1-\mathcal{P}^2)^{3/2}} + O(\gamma^2). \tag{F6}$$

Substituting the above results into Eqs. (55) and (69), we obtain

$$\mathcal{B} = \frac{2\mathcal{A}(1-\mathcal{P}^2)^{3/2}}{(\chi - \delta)}, \tag{F7}$$

substituting into Eqs. (56) and (70), we obtain

$$\mathcal{C} = -\mathcal{P}(2-\mathcal{P}^2) - \frac{3\mathcal{P}(1-\mathcal{P}^2)^2}{(\chi-\delta)^2}\mathcal{A}^2. \tag{F8}$$

These results can be used to calculate the corrections to the field variables $\overline{\mathcal{S}}$, and $\overline{\mathcal{A}}$ and the correction of the polarization $\overline{\mathcal{P}}$. Using Eq. (54) and comparing the γ^2 terms, we obtain

$$\overline{\mathcal{P}} = -\frac{(1-\mathcal{P}^2)^{3/2}}{(\chi-\delta)}\overline{\mathcal{S}}, \tag{F9}$$

and from Eq. (52) we obtain the differential equation

$$\frac{d^2\overline{\mathcal{S}}}{d\zeta^2} + (\chi^2 - \eta^2)\overline{\mathcal{S}} + 2(\chi - \eta)\overline{\mathcal{P}} = -(\chi - \eta)\mathcal{C} + \frac{d\mathcal{B}}{d\zeta}. \tag{F10}$$

The functions on the right-hand side of Eq. (F10) are known; substituting Eq. (F9) for $\overline{\mathcal{P}}$ we obtain, an inhomogeneous second order equation for $\overline{\mathcal{S}}$. We have solved this equation numerically, discretizing the functions and using a matrix inversion. Next using these results and substituting into Eq. (53), we obtain a differential equation for $\overline{\mathcal{A}}$:

$$\frac{d^2\overline{\mathcal{A}}}{d\zeta^2} + (\chi^2 - \eta^2)\overline{\mathcal{A}} = 2\frac{d\overline{\mathcal{P}}}{d\zeta} + (\eta + \delta)\mathcal{B} + \frac{d\mathcal{C}}{d\zeta} - 2\mathcal{A}\sqrt{1-\mathcal{P}^2} - \frac{\mathcal{P}\mathcal{A}\mathcal{S}}{\sqrt{1-\mathcal{P}^2}}. \tag{F11}$$

This is an inhomogeneous equation with constant coefficients. The right-hand side functions become known as soon as we calculate $\overline{\mathcal{P}}$.

[1] A.B. Aceves, C. De Angelis, and S. Wabnitz, Opt. Lett. **17**, 1566 (1992); B.A. Malomed and R.S. Tasgal, Phys. Rev. E **49**, 5787 (1994); I.V. Barashenkov, D.E. Pelinovsky, and E.V. Zemlyanaya, Phys. Rev. Lett. **80**, 5117 (1998); A. De Rossi, C. Conti, and S. Trillo, *ibid.* **81**, 85 (1998); A.R. Champneys, B.A. Malomed, and M.J. Friedman, *ibid.* **80**, 4169 (1998).

[2] B.J. Eggleton, R.E. Slusher, C.M. de Sterke, P.A. Krug, and J.E. Sipe, Phys. Rev. Lett. **76**, 1627 (1996); C.M. de Sterke, B.J. Eggleton, and P.A. Krug, J. Lightwave Technol. **15**, 1494 (1997).

[3] T. Peschel, U. Peschel, F. Lederer, and B.A. Malomed, Phys. Rev. E **55**, 4730 (1997); C. Conti, S. Trillo, and G. Assanto, Phys. Rev. Lett. **78**, 2341 (1997); Phys. Rev. E **57**, R1251 (1998); H. He and P.D Drummond, Phys. Rev. Lett. **78**, 4311 (1997); Phys. Rev. E **58**, 5025 (1998); S. Trillo and P. Ferro, Opt. Lett. **20**, 438 (1995); P. Drummond, H. He, and B.A. Malomed, Opt. Commun. **123**, 394 (1996); H. He, A. Arraf, C.M. de Sterke, P.D. Drummond, and B.A. Malomed, Phys. Rev. E **59**, 6064 (1999).

[4] A. Kozhekin and G. Kurizki, Phys. Rev. Lett. **74**, 5020 (1995).

[5] A.E. Kozhekin, G. Kurizki, and B. Malomed, Phys. Rev. Lett. **81**, 3647 (1998).

[6] S.L. McCall and E.L. Hahn, Phys. Rev. **183**, 457 (1969); Phys. Rev. A **2**, 861 (1970); A. C. Newell and J. V. Moloney, *Nonlinear Optics* (Addison-Wesley, Redwood City, CA, 1992).

[7] N. Aközbek and S. John, Phys. Rev. E **58**, 3876 (1998).

[8] Y.S. Kivshar and B. Luther-Davies, Phys. Rep. **298**, 81 (1998).

[9] A.A. Afanas'ev, V.M. Volkov, V.V. Dritz, and B.A. Samson,

J. Mod. Opt. **37**, 165 (1990); M.J. Shaw and B.W. Shore, J. Opt. Soc. Am. B **8**, 1127 (1991).

[10] B.I. Mantsyzov and R.N. Kuz'min, Zh. Eksp. Teor. Fiz. **91**, 65 (1986), [Sov. Phys. JETP **64**, 37 (1986)]; B.I. Mantsyzov, Phys. Rev. A **51**, 4939 (1995).

[11] H.G. Winful, J.H. Marburger, and E. Garmire, Appl. Phys. Lett. **35**, 379 (1979).

[12] G. Khitrova, H. M. Gibbs, F. Jahnke, M. Kira, and S. W. Koch, Rev. Mod. Phys. **71** (1999).